Published in final edited form as:
Cancer Discov. 2015 January ; 5(1): 35–42. doi:10.1158/2159-8290.CD-14-0621.

REAL-TIME INTRAVITAL IMAGING ESTABLISHES TUMOUR-ASSOCIATED MACROPHAGES AS THE EXTRASKELETAL TARGET OF BISPHOSPHONATE ACTION IN CANCER

Simon Junankar[1], **Gemma Shay**[2,7], **Julie Jurczyluk**[1], **Naveid Ali**[1], **Jenny Down**[1], **Nicholas Pocock**[1,3], **Andrew Parker**[4], **Akira Nguyen**[1], **Shuting Sun**[5], **Boris Kashemirov**[5], **Charles E. McKenna**[5], **Peter I. Croucher**[1], **Alexander Swarbrick**[1], **Katherine Weilbaecher**[6], **Tri Giang Phan**[1,8], and **Michael J. Rogers**[1,8]

[1]Garvan Institute of Medical Research and St Vincent's Clinical School, Faculty of Medicine, UNSW Australia, Sydney, Australia

[2]Division of Applied Medicine, University of Aberdeen, Aberdeen, UK

[3]Dept of Nuclear Medicine, St Vincent's Hospital, Sydney, Australia

[4]Dept of Pathology, St Vincent's Hospital, Sydney, Australia

[5]University of Southern California, Los Angeles, USA

[6]Dept of Medicine, Washington University School of Medicine, St Louis, USA

Abstract

Recent clinical trials have shown that bisphosphonate drugs improve breast cancer patient survival independent of their anti-resorptive effects on the skeleton. However, since bisphosphonates bind rapidly to bone mineral, the exact mechanisms of their anti-tumour action, particularly on cells outside of bone, remain unknown. Here we used real-time intravital two-photon microscopy to show extensive leakage of fluorescent bisphosphonate from the vasculature in 4T1 mouse mammary tumours, where it initially binds to areas of small, granular microcalcifications that are engulfed by tumour-associated macrophages (TAMs), but not tumour cells. Importantly, we also observed uptake of radiolabeled bisphosphonate in the primary breast tumour of a patient and showed the resected tumour to be infiltrated with TAMs and to contain similar granular microcalcifications. These data represent the first compelling *in vivo* evidence that bisphosphonates can target cells in tumours outside the skeleton and that their anti-tumour activity is likely to be mediated via TAMs.

Address for correspondence: Prof Mike Rogers, Garvan Institute of Medical Research, 384 Victoria St, Darlinghurst, Sydney, NSW 2010, Australia, m.rogers@garvan.org.au.
[7]Current address: H. Lee Moffitt Cancer Center, Tampa, USA.
[8]These senior authors contributed equally to the study.

Conflicts of interest: MJR has received research grants and honoraria from Novartis. SS co-affiliates with BioVinc, LLC (Culver City, CA USA). The other authors disclose no potential conflicts of interest.

Keywords

Bisphosphonate; macrophage; myeloid cell; TAM; AF647-RIS; ^{99m}Tc-MDP; zoledronic acid; ZOL; intravital two-photon microscopy

INTRODUCTION

For more than two decades, bisphosphonate (BP) drugs have been the frontline therapy for the treatment and prevention of skeletal-related events in cancer patients with multiple myeloma and bone metastases because they rapidly target the skeleton and inhibit osteoclastic bone resorption. In osteoclasts, nitrogen-containing BPs (N-BPs) such as zoledronic acid (ZOL) act intracellularly by inhibiting farnesyldiphosphate (FPP) synthase, a key enzyme in the mevalonate pathway. This prevents the biosynthesis of isoprenoids necessary for the prenylation, and hence membrane localisation and function, of small GTPases essential for osteoclastic bone resorption(1). Because of their high affinity for bone, the bioavailability of BPs in soft tissues is assumed to be very low. However, in various pre-clinical models, N-BPs have been shown to exert striking osteoclast-independent anti-tumour effects including on tumours located outside the skeleton(2). Indeed, several large clinical trials in patients with breast cancer and multiple myeloma have also indicated recently that N-BPs have benefits beyond inhibiting bone resorption(3). Zometa (zoledronic acid/ZOL) significantly increased disease-free survival when used alongside adjuvant endocrine therapies in women with early breast cancer(4) and in postmenopausal breast cancer patients when used as adjuvant therapy with aromatase inhibitors or other endocrine therapies(5, 6). Importantly, ZOL also decreased the loco-regional recurrence of tumours outside the skeleton(5). These findings are supported by several meta-analyses indicating significant benefits in disease-free and overall survival as well as decreased local and distant tumour recurrence. Moreover, epidemiological studies also suggest that long-term BP therapy decreases the risk of invasive breast cancer(7). Nevertheless, there is ongoing controversy over whether N-BPs exert direct or indirect anti-tumour effects *in vivo* and the cellular targets and mechanisms involved, particularly in cells outside the skeleton, have yet to be elucidated. Furthermore, ^{99m}technetium-labelled methylene bisphosphonate (^{99m}Tc-MDP, a radionuclide bone scanning agent commonly used to detect bone metastases), is recognised to accumulate in some extraskeletal tumours, including neuroblastomas, sarcomas and breast carcinomas, although its exact mechanism of uptake in soft-tissue tumours is unclear(8). MDP is the simplest chemical form of BP and, like N-BPs, binds avidly to calcium ions and is internalised into cells by endocytosis. Therefore, to determine how BPs localise to soft-tissue tumours to exert their anti-tumour activity, we used intravital two-photon microscopy, together with flow cytometric analysis, to determine the cell types capable of internalising a fluorescently-labelled N-BP in a soft tissue tumour model. We used the syngeneic 4T1 mouse model of breast cancer since treatment with ZOL has previously been shown to reduce visceral metastases in this model(9). Finally, to confirm our findings, we analysed the uptake of ^{99m}Tc-MDP by the primary breast tumour in the pre-operative bone scan of a patient and examined the post-operative resected tumour for microcalcifications and infiltration by TAMs.

RESULTS

N-BP accumulates in mammary tumour tissue via leaky tumour vasculature

To identify the cell types capable of internalising N-BP in tumours outside the skeleton and the route of cellular uptake, we fluorescently conjugated the N-BP rise dronate to form a bone-seeking but pharmacologically inactive analogue (AF647-RIS)(12) and examined its localisation in mice bearing syngeneic 4T1 mammary tumours. Infra-red imaging of tumour explants 24 hours after subcutaneous injection showed that AF647-RIS was detectable in whole 4T1 mammary tumours (Supplementary Fig S1A) where it localised to the tumour periphery (Supplementary Fig S1B). Two-photon imaging of tumour explants revealed that AF647-RIS was present intracellularly in cells located in and beneath the tumour capsule (Supplementary Fig S1C), a region enriched for F4/80^{+} tumour-associated macrophages (TAMs) (Supplementary Fig S1D and 1E).

Based on these observations, we next examined the dynamic distribution and cellular uptake of AF647-RIS in real-time in 4T1 mammary tumours of live mice using intravital two-photon microscopy. Prior to imaging, TAMs were labelled *in vivo* with anti-F4/80 monoclonal antibody (mAb) conjugated to FITC. Imaging of second-harmonic generation (SHG) by collagen fibres revealed that tumours were supplied by a dense, subcapsular network of tortuous capillaries and small blood vessels closely associated with F4/80^{+} TAMs (Fig. 1A and Supplementary Movie 1). Immediately following intravenous injection, AF647-RIS could be visualised flowing into the vascular bed of the mammary tumours and leaking into the surrounding tumour tissue. In contrast, intravital imaging of the normal mammary fat pad of mice that did not receive 4T1 tumour cells showed rapid transit of AF647-RIS through the blood vessels in <5 minutes and absence of any capillary leak into mammary tissue (Fig 1A, 1B and Supplementary Movie 2). The same findings were obtained using the fluorescently-labelled N-BP pamidronate (OsteoSense 680). Thus, contrary to dogma, BPs are able to access extraskeletal tumours because of the well-documented leaky new blood vessels that form in tumours(13).

Tumour-associated macrophages phagocytose N-BP-coated microcalcifications

Unbound AF647-RIS persisted in 4T1 tumour blood vessels and mammary tumour tissue for >15 minutes after injection of mice (Fig. 1A, 1B) and was observed to rapidly (within minutes) bind 2–5μm granular clumps. These micro-structures were calcified, since they bound the calcium-seeking dye calcein*in vivo* as well as N-BP (Fig 2A). Image analysis of a 425×425×150μm volume (ie 51 optical sections) of tumour showed that 43% of N-BP colocalised with calcein, with a Pearson's correlation of 0.4 (Supplementary Fig. S2). These structures closely resembled the small granules of microcalcification (distinct from the larger calcifications present in the lumen of mammary ducts) that we detected histologically in sections of random human breast cancer tissue by von Kossa staining (Fig 2Bi,ii). In an additional 40 samples of human breast tumour tissue, 40% showed evidence of these small, granular microcalcifications(3/10 ER^{+} tumours, 4/10 ER^{+}Her2^{+} tumours, 2/10 ER^{-}Her2^{+} tumours, 7/10 triple negative tumours).

Importantly, in mice with 4T1 mammary tumours, F4/80$^+$ TAMs were observed to bind and internalise small, subcellular complexes of AF647-RIS by pinocytosis (Fig. 3A and Supplementary Movie 3), whereas AF647-RIS bound to microcalcified granules was engulfed by phagocytosis (Fig. 3B and Supplementary Movie 4). Notably we did not observe any uptake in any non-F4/80-labeled cells such as epithelial cells. Imaging of mice 24h following AF647-RIS administration indicated that the bulk of the AF647-RIS was localised in the cytoplasm of F4/80$^+$ cells, confirming the uptake by TAMs (Fig 3C and Supplementary Movie 5).

We also examined the uptake of fluorescently-labelled N-BP in mice bearing subcutaneous B16. F10 melanomas. Whilst we also observed some leakage of N-BP from tumour capillaries, in contrast to 4T1 tumours we did not observe any binding to granular calcifications or retention of N-BP in the tumour tissue (Supplementary Figure S3A). Although we did detect some calcein staining in the B16 tumours, this was considerably less than in the 4T1 tumours (Supplementary Figure S3B). Consistent with this, FACS analysis showed little uptake of N-BP by TAMs in B16 tumours (Supplementary Figure S3C). This suggests that the presence of microcalcifications in tumours strongly enhances the efficiency of uptake of N-BP by TAMs.

N-BP is efficiently internalised in vivo by tumour-associated macrophages but not by tumour cells

To confirm the phenotype of the cells responsible for uptake of N-BP, we performed multiparameter flow cytometric analysis of enzymatically-digested, single cell suspensions of tumours. 4T1 tumours consisted of a large infiltrate of immune cells, with about 50% of the cells being CD45$^+$ tumour-infiltrating leukocytes (Fig. 3D). There was minor uptake of AF647-RIS by EpCAM$^+$ mammary epithelial cells (Fig. 3E), with a small shift in mean fluorescence intensity (MFI) that was below the limit of detection of our intravital imaging modalities (Fig. 1A, 1B). The bulk of AF647-RIS, however, was taken up by a major subpopulation of CD45$^+$ leukocytes (Fig. 3E). Analysis for F4/80 expression confirmed these cells were F4/80$^+$ TAMs (Fig. 3F, 3G), confirming the results of the intravital imaging studies (Fig 3C and Supplementary Movie 5). Significantly, quantification of the MFI showed a near 5-fold increase in AF647-RIS MFI in CD45$^+$ F4/80$^+$ TAMs compared to <2-fold increase in tumour epithelial cells and no increase in CD45$^+$ F4/80^{neg} tumour-infiltrating leukocytes (Fig. 3G, 3H). Further analysis showed that the F4/80$^+$ TAMs that internalised AF647-RIS were also CD11b$^+$ (Fig. 3I). Collectively these data identify TAMs as the cell type targeted by N-BP in mammary tumours.

Clinicopathological correlation of bisphosphonate uptake in human breast cancer with microcalcifications and tumour-associated macrophages

A 51-year old female patient presented with a grade 1 invasive duct carcinoma associated with ductal carcinoma *in-situ* and focal lymphovascular invasion (whole tumour size 16mm). A routine bone scintigraphy scan using ^{99m}Tc-MDP and multimodal SPECT/CT imaging revealed clear uptake of the radionuclidein the mammary carcinoma (Fig. 4A). Sections of the resected tumour of this patient showed extensive CD68$^+$ and CD163$^+$macrophage infiltration (Fig. 4B, i, ii). Furthermore, von Kossa staining revealed

the presence of small, granular calcifications within the mammary tumour tissue (Fig. 4B, iii), and in adjacent benign tissue (Fig. 4B, iv, v), that were similar in size and appearance to those observed to bind N-BP and be internalised by TAMs in the mouse 4T1 tumours. Some of these granular microcalcifications in the human tumour tissue were also closely associated with, or even appeared to have been internalised by, $CD68^+$ or $CD163^+$macrophages (Fig. 4B, ii/iii, iv/v).

DISCUSSION

The exact mechanism underlying the *in vivo* anti-tumour activity of N-BPs has been highly controversial because it is not clear which cell types internalise these drugs in tumours, particularly outside the skeleton. Other studies have shown that N-BP treatment can affect the mevalonate pathway in subcutaneous or peritoneal tumours in mouse models *in vivo*, but these reports did not identify the exact cell types involved(16–18). Our data show unequivocally that, in 4T1 mammary tumours, N-BP is rapidly and efficiently internalised by TAMs rather than tumour cells. This is consistent with reports that ZOL treatment reduces the number of TAMs in mouse models of mammary and cervical cancer(19, 20). It appears that TAMs have a selective ability to internalise N-BPs that is shared with other myeloid lineage cells such as peripheral blood and bone marrow monocytes, peritoneal macrophages and osteoclasts(21) and is most likely related to the capacity of these cells for pinocytosis and phagocytosis of calcium-containing complexes (such as microcalcifications), since there is no evidence for any other specific transport mechanisms for cellular uptake of these drugs(22). Indeed, engulfment of N-BP-coated microcalcifications may be the major route of uptake by TAMs *in vivo* since we observed little uptake of N-BP by TAMs in B16 tumours that lacked extensive binding of N-BP to microcalcifications.

Small, granular microcalcifications are common in human breast tumours since we identified their presence in 40% of the tissue samples examined. In mouse 4T1 tumours, microcalcified granules were also found to be present throughout the tumour tissue; the particular localization and retention of AF647-RIS in the tumour periphery presumably reflects the high density of leaky vessels in this region. The time-course of the distribution and cellular uptake of AF647-RIS in 4T1 tumours (within 30 minutes of injection) is entirely consistent with the rapid localisation of ^{99m}Tc-MDP in breast tumours observed in some patients by scintigraphic imaging(14). Our observations therefore identify the likely mechanism of soft-tissue tumour localisation of ^{99m}Tc-MDP in humans, by a similar mechanism to that observed in mice ie via leaky tumour vessels and binding to granular microcalcifications that are engulfed by TAMs. This provides a mechanistic explanation for a phenomenon that was first described 40 years ago(15) but remains poorly characterised.

In osteoclasts and macrophages, inhibition of FPP synthase by N-BPs and the subsequent loss of prenylation of small GTPases affects numerous processes including polarisation, adhesion, migration, vesicular trafficking, proliferation and survival(1, 23). It is highly likely that N-BP treatment also affects multiple functions of TAMs *in vivo* by inhibiting protein prenylation. TAMs have emerged as powerful promoters of tumour growth and metastasis(24) and extensive macrophage infiltration in many tumour types is associated

with poor patient prognosis(25). Our studies indicate that the anti-tumour activity of N-BPs observed in preclinical models and in clinical trials is likely mediated indirectly through uptake of these drugs by TAMs and possibly other myeloid lineage cells, leading to their functional impairment and depletion, rather than by direct effects on tumour cells *per se*. These observations provide a further rationale for the use of N-BP as adjuvant cancer therapy in patients with early stage disease.

MATERIALS AND METHODS

SPECT/CT imaging of patients

Radionuclide bone scans were performed using 900MBq ^{99m}Tc-MDP (technetium-99m-methylene diphosphonate; RadPharm) followed by multimodal SPECT/CT imaging after 3 hours using a GE Discovery NM/CT 670 with BrightSpeed Elite16 slice CT and Advanced Elite NXT SPECT detectors.

Preclinical mouse tumour models

Immunocompetent BALB/c mice aged 6-to-8 weeks were obtained from Australian BioResources (Moss Vale, Australia) and housed at the Garvan Institute of Medical Research, 4T1-Luc2 cells were purchased from Perkin Elmer (MA, USA) and used within 6 months without authentication. For tumour transplantation, 4T1 cells were resuspended in PBS and 5×10^5 cells in a 10μl volume were injected into the 4th inguinal mammary fat pad. B16. F10 cells were purchased from American Type Culture Collection (Manassas, VA 20108 USA) and used within 6 months (passage 2). 2×10^6 cells in a 50μl volume were inoculated subcutaneously into the flanks of C57/Bl6 mice. Mice were administered a single dose of N-BP (0.9mg/kg AF647-RIS or 0.7mg/kg OsteoSense 680) or 70mg/kg calcein 10–14 days after tumour cell inoculation.

Intravital two-photon microscopy of 4T1 mammary tumours

We used a Zeiss 7MP two-photon microscope (Carl Zeiss, Germany) excited by a Chameleon Vision II Ti:Sa laser (Coherent Scientific, Australia) with filters and detectors as described previously(10). Intravital two-photon microscopy of mammary fat pad and 4T1 tumours was based on the method for imaging the medullary surface of inguinal lymph nodes(11). See Supplementary Methods for additional details.

Flow cytometry

Mice with palpable mammary tumours received a single subcutaneous injection of N-BP (0.9 mg/kg AF647-RIS or 0.7mg/kg OsteoSense 680). 24 hours later the mice were perfused with PBS and euthanased. Tumours were mechanically dispersed and enzymatically digested (Collagenase Blend L, Sigma, MO, USA) using a gentle MACS (Milltenyi Biotech, Bergisch Gladbach, Germany) tissue dissociator, incubated with DNase (1mg/ml, Sigma), then passed through a 70μm nylon strainer (BD Biosciences, MA, USA). Erythrocytes were lysed using ammonium chloride, the remaining cells were washed once in PBS, blocked with anti-CD16/32 (eBioscience, CA, USA) for 10 minutes on ice, then stained with antibodies to CD45 (APC-AF750, from eBioscience, CA, USA), F4/80 (FITC, from UCSF Hybridoma Core Facility), and EpCAM (PerCP-Cy5.5, from Biolegend, CA, USA), prior to

analysis on a LSRII SORP flow cytometer using BD FACS DIVA software. Data were analysed using FlowJo software (TreestarInc, OR, USA). For detection of AF647-RIS uptake, cells from the tumours of vehicle-treated animals were used as controls for background fluorescence. Fluorescence due to AF647-RIS uptake was measured as the geometric mean in the R670nm channel, in $CD45^{+}EpCAM^{-}$ or $CD45^{-}EpCAM^{+}$ populations.

Histology

Ethics approval was granted for the use of pathology specimens and cognate clinicopathological data (Human Research Ethics Committee of St Vincent's Hospital, Sydney, NSW, Australia). For von Kossa staining of microcalcifications, 5μm FFPE sections of tumour were dewaxed and hydrated with distilled water then incubated in 1% silver nitrate in bright light for 1 hour. Sections were then incubated in 5% sodium thiosulphate for 5 minutes and counterstained with 1% toluidine blue for 30 seconds. Slides were then dehydrated and cleared before mounting in Eukitt. Serial sections were immunostained for CD163 (clone 10D6, Novocastra) or CD68 (Ventana predilute KP1 antibody) using a standard protocol on a Ventana XT machine with CC1 antigen retrieval, brown chromogen and haematoxylin counterstain. Images were captured using a Leica DM 6000 Power Mosaic microscope with a DFC310FX camera. See Supplementary methods for additional details of immunostaining.

Ethical statement

Written, informed consent was obtained from the patient for the use of de-identified SPECT/CT images. Animal experiments were approved by the Garvan Institute of Medical Research/St. Vincent's Hospital Animal Experimentation Ethics Committee(AEC 12_41).

Statistics

Unpaired, two-sided student's t-test with Welch's correction was performed using Prism software (GraphPad, CA, USA).

Supplementary Material

Refer to Web version on PubMed Central for supplementary material.

Acknowledgments

Financial Support: This work was funded by project grant RG 14–12 from Cancer Council NSW (MJR and TGP). TGP was also supported by a Career Development Fellowship and Project Grants from the NHMRC and KW was supported by RO1-CA097250. GS was funded by a studentship from the Fraserburgh Moonlight Prowl, facilitated by Prof S. Heys, University of Aberdeen.

GRANT SUPPORT

This work was funded by project grant RG 14–12 from Cancer Council NSW to MJR and TGP. TGP was also supported by a Career Development Fellowship and Project Grants from the NHMRC and KW was supported by RO1-CA097250. GS was funded by a studentship from the Fraserburgh Moonlight Prowl, facilitated by Prof S. Heys, University of Aberdeen. Tissues and samples were received from the Australia Breast Cancer Tissue Bank which is generously supported by the National Health and Medical Research Council of Australia, The Cancer Institute NSW and the National Breast Cancer Foundation.

We thank Dr Hal Ebetino for his support in the development of fluorescent bisphosphonates for *in vivo* imaging, Mehreen Arshi, Mary Hornick, Natasa Kovacic and Michelle Mcdonald for technical assistance, Prof. Antony Basten for comments on the manuscript and Tyani Chan for proofreading.

References

1. Rogers MJ, Crockett JC, Coxon FP, Monkkonen J. Biochemical and molecular mechanisms of action of bisphosphonates. Bone. 2011; 49:34–41. [PubMed: 21111853]
2. Clezardin P. Bisphosphonates' antitumor activity: an unravelled side of a multifaceted drug class. Bone. 2011; 48:71–9. [PubMed: 20655399]
3. Coleman R, Gnant M, Morgan G, Clezardin P. Effects of bone-targeted agents on cancer progression and mortality. J Natl Cancer Inst. 2012; 104:1059–67. [PubMed: 22752060]
4. Gnant M, Mlineritsch B, Schippinger W, Luschin-Ebengreuth G, Postlberger S, Menzel C, et al. Endocrine therapy plus zoledronic acid in premenopausal breast cancer. N Engl J Med. 2009; 360:679–91. [PubMed: 19213681]
5. Coleman RE, Marshall H, Cameron D, Dodwell D, Burkinshaw R, Keane M, et al. Breast-cancer adjuvant therapy with zoledronic acid. N Engl J Med. 2011; 365:1396–405. [PubMed: 21995387]
6. Coleman R, de Boer R, Eidtmann H, Llombart A, Davidson N, Neven P, et al. Zoledronic acid (zoledronate) for postmenopausal women with early breast cancer receiving adjuvant letrozole (ZO-FAST study): final 60-month results. Annals of oncology : official journal of the European Society for Medical Oncology/ESMO. 2013; 24:398–405. [PubMed: 23047045]
7. Chlebowski RT, Chen Z, Cauley JA, Anderson G, Rodabough RJ, McTiernan A, et al. Oral bisphosphonate use and breast cancer incidence in postmenopausal women. JClin Oncol. 2010; 28:3582–90. [PubMed: 20567009]
8. Worsley DF, Lentle BC. Uptake of technetium-99m MDP in primary amyloidosis with a review of the mechanisms of soft tissue localization of bone seeking radiopharmaceuticals. J Nucl Med. 1993; 34:1612–5. [PubMed: 8355083]
9. Hiraga T, Williams PJ, Ueda A, Tamura D, Yoneda T. Zoledronic acid inhibits visceral metastases in the 4T1/luc mouse breast cancer model. Clin Cancer Res. 2004; 10:4559–67. [PubMed: 15240548]
10. Chtanova T, Hampton HR, Waterhouse LA, Wood K, Tomura M, Miwa Y, et al. Real-time interactive two-photon photoconversion of recirculating lymphocytes for discontinuous cell tracking in live adult mice. Journal of Biophotonics. 2014; 7:425–33. [PubMed: 23184395]
11. Grigorova IL, Schwab SR, Phan TG, Pham TH, Okada T, Cyster JG. Cortical sinus probing, S1P1-dependent entry and flow-based capture of egressing T cells. Nature Immunology. 2009; 10:58–65. [PubMed: 19060900]
12. Roelofs AJ, Coxon FP, Ebetino FH, Lundy MW, Henneman ZJ, Nancollas GH, et al. Fluorescent risedronate analogues reveal bisphosphonate uptake by bone marrow monocytes and localization around osteocytes in vivo. J Bone Miner Res. 2010; 25:606–16. [PubMed: 20422624]
13. McDonald DM, Baluk P. Significance of blood vessel leakiness in cancer. Cancer Research. 2002; 62:5381–5. [PubMed: 12235011]
14. Piccolo S, Lastoria S, Mainolfi C, Muto P, Bazzicalupo L, Salvatore M. Technetium-99m-methylene diphosphonate scintimammography to image primary breast cancer. J Nucl Med. 1995; 36:718–24. [PubMed: 7738640]
15. Berg GR, Kalisher L, Osmond JD, Pendergrass HP, Potsaid MS. 99mTc-diphosphonate concentration in primary breast carcinoma. Radiology. 1973; 109:393–4. [PubMed: 4355069]
16. Guenther A, Gordon S, Tiemann M, Burger R, Bakker F, Green JR, et al. The bisphosphonate zoledronic acid has antimyeloma activity in vivo by inhibition of protein prenylation. IntJ Cancer. 2010; 126:239–46. [PubMed: 19621390]
17. Ottewell PD, Lefley DV, Cross SS, Evans CA, Coleman RE, Holen I. Sustained inhibition of tumor growth and prolonged survival following sequential administration of doxorubicin and zoledronic acid in a breast cancer model. IntJ Cancer. 2010; 126:522–32. [PubMed: 19621384]
18. Benzaid I, Monkkonen H, Bonnelye E, Monkkonen J, Clezardin P. In vivo phosphoantigen levels in bisphosphonate-treated human breast tumors trigger Vgamma9Vdelta2 T-cell antitumor

cytotoxicity through ICAM-1 engagement. Clinical Cancer Res. 2012; 18:6249–59. [PubMed: 23032740]

19. Melani C, Sangaletti S, Barazzetta FM, Werb Z, Colombo MP. Amino-biphosphonate-mediated MMP-9 inhibition breaks the tumor-bone marrow axis responsible for myeloid-derived suppressor cell expansion and macrophage infiltration in tumor stroma. Cancer Res. 2007; 67:11438–46. [PubMed: 18056472]
20. Giraudo E, Inoue M, Hanahan D. An amino-bisphosphonate targets MMP-9-expressing macrophages and angiogenesis to impair cervical carcinogenesis. J Clin Invest. 2004; 114:623–33. [PubMed: 15343380]
21. Roelofs AJ, Thompson K, Ebetino FH, Rogers MJ, Coxon FP. Bisphosphonates: Molecular Mechanisms of Action and Effects on Bone Cells, Monocytes and Macrophages. Curr Pharm Des. 2010; 16:2950–60. [PubMed: 20722616]
22. Thompson K, Rogers MJ, Coxon FP, Crockett JC. Cytosolic entry of bisphosphonate drugs requires acidification of vesicles after fluid-phase endocytosis. Mol Pharmacol. 2006; 69:1624–32. [PubMed: 16501031]
23. Itzstein C, Coxon FP, Rogers MJ. The regulation of osteoclast function and bone resorption by small GTPases. Small GTPases. 2011; 2:117–30. [PubMed: 21776413]
24. Joyce JA, Pollard JW. Microenvironmental regulation of metastasis. Nature Rev Cancer. 2009; 9:239–52. [PubMed: 19279573]
25. Bingle L, Brown NJ, Lewis CE. The role of tumour-associated macrophages in tumour progression: implications for new anticancer therapies. J Pathol. 2002; 196:254–65. [PubMed: 11857487]

SIGNIFICANCE

Bisphosphonates are assumed to act solely in bone. However, mouse models and clinical trials show that they have surprising anti-tumour effects outside bone. We provide unequivocal evidence that bisphosphonates target TAMs but not tumour cells to exert their extraskeletal effects, offering a rationale for use in patients with early disease.

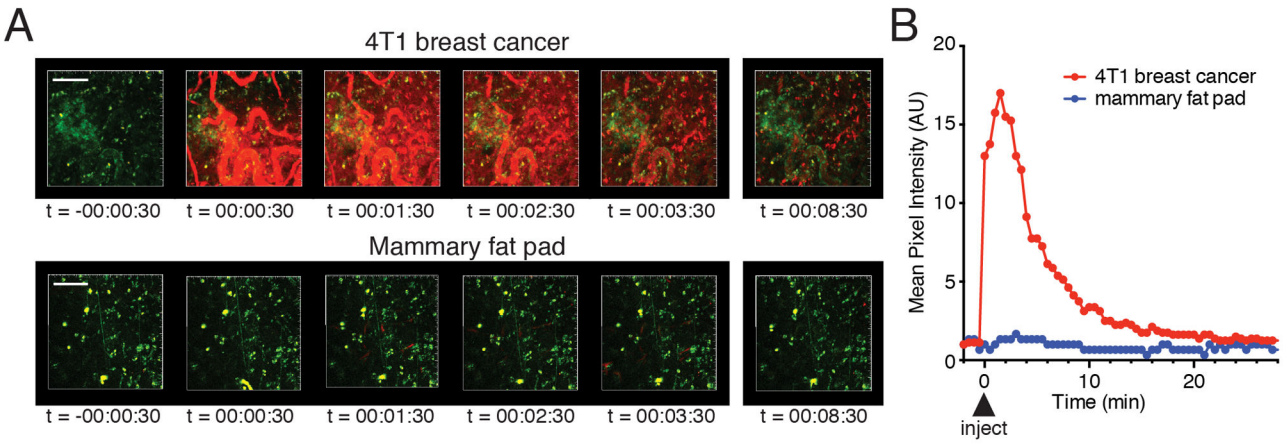

Fig 1. Dynamic *in vivo* distribution and cellular uptake of AF647-RIS in 4T1 mammary tumours

(A) Time-lapse 72μm maximal intensity projections from the tissue surface of 4T1 breast tumour (upper panel) and normal mammary fat pad (lower panel), imaged by intravital two-photon microscopy (red = AF647-RIS, green = F4/80; the second harmonic generation signal from subcapsular collagen has been removed for clarity). Images correspond to Supplementary Movie 1 and 2. (B) Quantification of tissue distribution of AF647-RIS from (A). Time stamp indicates hh:mm:ss after injection of AF647-RIS. Scale bar = 100μm. Data are representative of 3 independent experiments.

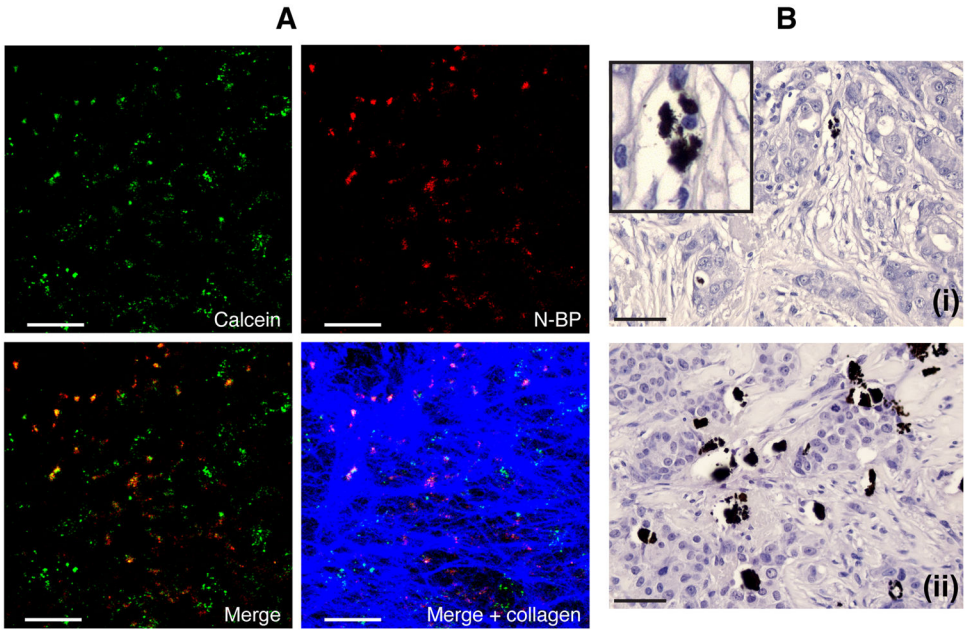

Fig 2. Detection of microcalcifications in 4T1 mammary tumours and human breast tumour tissue

(A) Two-photon imaging of whole 4T1 tumour explants 16 hours after injection of mice with calcein and N-BP shows the presence of microcalcifications labelled *in vivo* with calcein (green) or OsteoSense 680 (purple), or both (orange in the merged image). Collagen in the tumour capsule is shown in blue. (B) Von Kossa staining detects small, granular microcalcifications in sections of tumour from two different patients, (i) and (ii), with triple negative disease (inset shows a magnified region from the same section). Scale bars = 50μm.

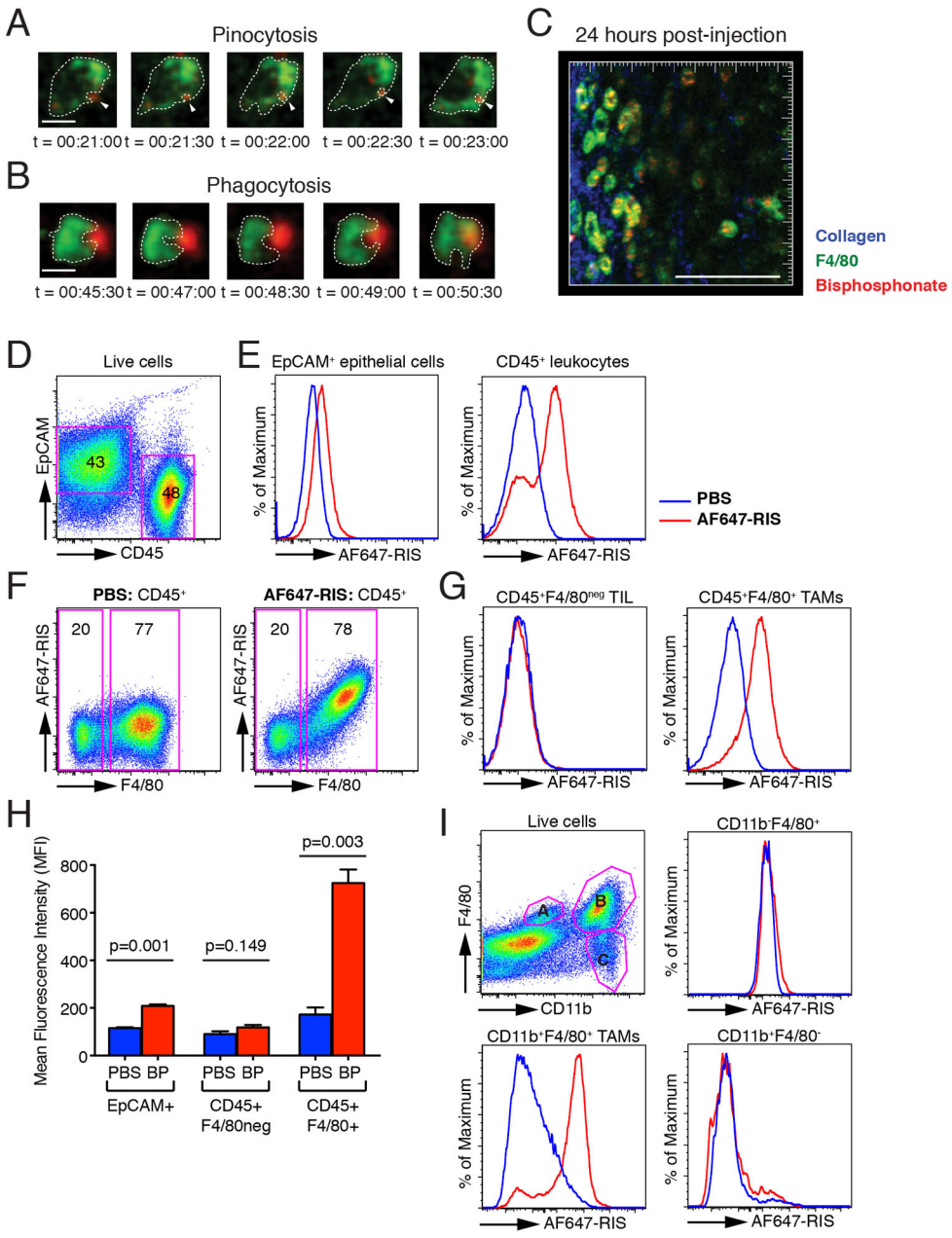

Fig 3. AF647-RIS is internalised by tumour-associated macrophages *in vivo*

(A)/(B) Time-lapse images from a single optical plane showing uptake of (A) small and (B) large AF647-RIS complexes (red) by F4/80-labelled macrophages (green); images correspond to Supplementary Movie 3 and 4 and are representative of 3independent experiments, with at least 3 single cells analysed per experiment. (C) 60μm maximal intensity projection from the surface of 4T1 breast tumour 24h after injection of AF647-RIS. Blue = collagen, green = F4/80, red = AF647-RIS; images correspond to Supplementary Movie 5. Scale bar = 10μm in (A) and (B), and 100μm in (C). Time stamp indicates hh:mm:ss after injection of AF647-RIS. (D) FACS staining of mammary epithelial cells for EpCAM and tumour-infiltrating leukocytes for CD45. (E) Histogram showing AF647-RIS

signal in mammary epithelial cells and tumour-infiltrating leukocytes (TIL) in mice treated with PBS (blue) or AF647-RIS (red). (F) Pseudocolour plot showing AF647-RIS and F4/80 gated on $CD45^+$ cells in mice treated with PBS (left) or AF647-RIS (right). (G) Histogram showing AF647-RIS signal in $CD45^+F4/80^{neg}$ TIL and $CD45^+F4/80^+$ TAMs in mice treated with PBS (blue) or AF647-RIS (red). (H) Quantification of AF647-RIS (BP) uptake. (I) FACS analysis of AF647-RIS (red) or PBS (blue) uptake by subpopulations of $F4/80^+$ TAMs. Data are the mean +/− SEM and are representative of at least 2 independent experiments with n=3 mice in each group.

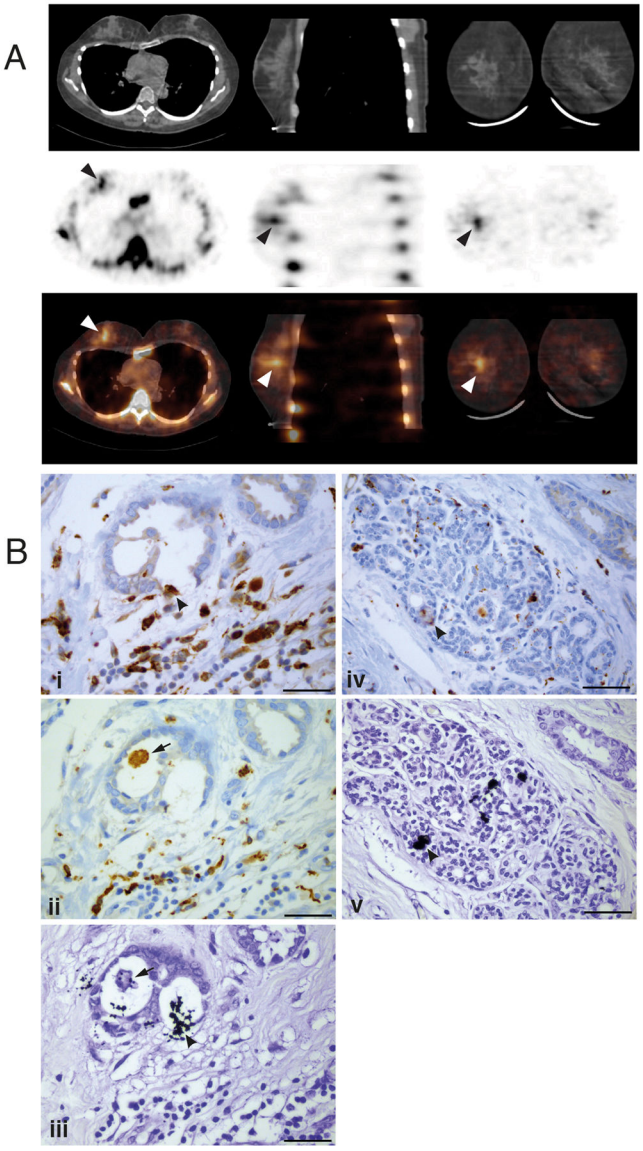

Fig. 4. Detection of ^{99m}Tc-MDP and microcalcificationsin human breast tumour

(A) The CT (upper panel), SPECT (middle panel) and combined SPECT/CT (lower panel) images show increased ^{99m}Tc-MDP uptake (arrowheads) in the right breast, corresponding to the carcinoma visible in the CT slice. (B) Following surgery, serial sections of the tumour from the same patient showed the presence of extensive CD68$^+$(i,iv) and CD163$^+$ (ii) macrophage infiltration. Serial sections stained with von Kossa reagent revealed small, granular microcalcifications (black) within the tumour tissue (iii) and in adjacent benign tissue (v), sometimes closely associated with CD68$^+$ macrophages; arrowheads show colocalisation of black calcifications and brown CD68$^+$ staining in (i)/(iii) and (iv)/(v). The arrow in (ii)/(iii) shows a CD163$^+$ macrophage that appears to contain intracellular microcalcifications. Scale bars = 50μm.